A comparative study of super- and highly-deformed bands in the $A \sim 60$ mass region

A. V. Afanasjev[1,2,3], I. Ragnarsson[3], P. Ring[1]

[1] *Physik-Department der Technischen Universität München, D-85747 Garching, Germany,*

[2]*Nuclear Research Center, Latvian Academy of Sciences, LV-2169, Salaspils, Miera str. 31,*

Latvia,

[3]*Department of Mathematical Physics, Lund Institute of Technology, PO Box 118, S-22100,*

Lund, Sweden

Abstract

Super- and highly-deformed rotational bands in the $A \sim 60$ mass region are studied within cranked relativistic mean field theory and the configuration-dependent shell-correction approach based on the cranked Nilsson potential. Both approaches describe the experimental data well. Low values of the dynamic moments of inertia $J^{(2)}$ compared with the kinematic moments of inertia $J^{(1)}$ seen both in experiment and in calculations at high rotational frequencies indicate the high energy cost to build the states at high spin and reflect the limited angular momentum content in these configurations.

Typeset using REVTEX

Extremely fast rotating nuclei are interesting laboratories providing information for test of theoretical models at extreme conditions (large angular momentum and/or deformation, limit of angular momentum in the rotational bands etc.). A special feature at the high rotational frequencies is that pairing correlations are considerably quenched and can often be neglected. A most interesting nuclear region is the one with $A \sim 60$ ($N \approx Z \approx 30$), where a large variety of rotational structures such as (smooth) terminating bands, highly-deformed and superdeformed (SD) rotational bands are expected to be observed up to very high rotational frequencies in the same nucleus. The ^{62}Zn nucleus [1,2] represents a first example of this variety.

Of special interest are the properties of SD bands in this region since they extend to the highest rotational frequencies (~ 1.8 MeV) observed so far in SD bands. The fact that the predicted SD band in the doubly-magic superdeformed nucleus ^{60}Zn [3] has been observed [4] and that it is linked to the low-spin level scheme is another attractive point. This is because by means of an effective alignment (or similar) approach [5,6], it becomes possible to map not only relative spin values as in the $A \sim 140 - 150$ mass region (see Refs. [6,7]) but also absolute spin values in the unlinked SD and highly-deformed bands. Then, in SD bands with little influence of pairing correlations, it will be possible to make a comparison between experiment and theory, not only for those physical observables which can be extracted without knowing absolute spin values (like dynamic moment of inertia $J^{(2)}$ and the transition quadrupole moment Q_t) but also, for the first time, for observables which cannot be extracted without such a knowledge (like the kinematic moment of inertia $J^{(1)}$ and the evolution of the excitation energy within a band as a function of spin).

In the present article, a comparative study of the recently observed highly-deformed band in ^{58}Cu [8] and the SD bands in ^{60,62}Zn [1,4] is presented. In addition, the general features of SD and highly-deformed bands in this mass region of $A \sim 60$ are outlined. Our theoretical tools are the cranked relativistic mean field theory (further CRMF) [9,10] and the configuration-dependent shell-correction approach based on the cranked Nilsson potential (further CN) [11,12].

In relativistic mean field (RMF) theory the nucleus is described as a system of point-like nucleons represented by Dirac-spinors and coupled to mesons and to the photon. The nucleons interact by the exchange of several mesons, namely, the scalar σ and three vector particles ω, ρ and the photon. The CRMF theory represents the extension of relativistic

mean field (RMF) theory to the rotating frame. CRMF theory is a fully self-consistent theory. On the contrary, in the CN model the total energy is described as a sum of the rotating liquid drop energy and the shell correction energy. This leaves some room for inconsistencies between macroscopic and microscopic parts as illustrated for example in Refs. [13,14]. However, it is commonly accepted that the CN model provides a reasonable description of the nuclear many-body problem. Both models have been very successful in describing different aspects of SD bands in the $A \sim 140 - 150$ mass region (see e.g. [7,15] and [6,13]). The details of the formalisms of these two approaches can be found in Refs. [7,15] and in Refs. [11,12], respectively.

CRMF calculations have been performed with three parameterizations of the RMF Lagrangian (NL1 [16], NL3 [17] and NLSH [18]) in order to define the force best suited for the description of rotational properties of the nuclei with $N \approx Z$. Since the results with NL3 are rather close to the ones with NLSH, they are not shown in some figures. The spatial components of the vector mesons (*nuclear magnetism*) play an extremely important role for the description of moments of inertia [19]. They are taken into account in a fully self-consistent way.

The relativistic mean field equations are solved in the basis of a deformed harmonic oscillator. A basis deformation of $\beta_0 = 0.2$ has been used. All bosonic states below the energy cutoff $E_B^{cut-off} \leq 16.5\hbar\omega_0^B$ and all fermionic states below the energy cutoff $E_F^{cut-off} \leq 13.5\hbar\omega_0^F$ have been used in the diagonalization. The increase of the fermionic space compared with the truncation scheme used in Ref. [7] was necessary because in the present study, we compare experimental and calculated excitation energies relative to rigid rotor reference which requires high accuracy in the calculation of energies. Note, however, that the energy cutoff $E_F^{cut-off} \leq 11.5\hbar\omega_0^F$ provides a rather good description of moments of inertia and the quadrupole and hexadecupole moments and thus it can be used for a more systematic investigations.

In the CN calculations, the standard set of the parameters for the Nilsson potential [11] has been used. In both approaches, pairing correlations are not taken into account. Therefore, the results can be considered as realistic only in the region of high spins, say $I \geq 15\hbar$. However, for some configurations the paired band crossings at low spin will be blocked and thus, in these cases, the results of the calculations are not expected to deviate significantly from experiment even at lower spin values; for details see the discussion in Ref.

[15]. To label the configurations we use the shorthand notation $[p_1 p_2, n_1 n_2]$ where p_1 (n_1) is the number of proton (neutron) $f_{7/2}$ holes and p_2 (n_2) is the number of proton (neutron) $g_{9/2}$ particles. Superscripts to the orbital labels are used to indicate the sign of signature r ($r = \pm i$) of the orbital.

According to the CRMF and the CN approaches, the doubly-magic SD band in ^{60}Zn has a $[22, 22]$ structure in the notation defined above. In this configuration, all single-particle levels below the $Z = N = 30$ SD shell gaps are occupied (see Fig. 1). At the spins of interest, this band is well separated from excited SD configurations (see Fig. 3 in Ref. [4]). The experimental observables ($J^{(1)}$, $J^{(2)}$ at $\Omega_x \geq 1.1$ MeV and Q_t) are well described in both approaches (see Figs. 2c,d and 4). At $\Omega_x \sim 0.95$ MeV, the observed band undergoes a paired band crossing, the description of which is not addressed in the present calculations. Note that this is a $N = Z$ nucleus, so the proton-neutron pairing correlations could play some role at high spin.

Contrary to ^{60}Zn, the bands in ^{58}Cu and ^{62}Zn are not linked to the low-spin level scheme and thus their parities and spins are not known experimentally. Considering the available single-particle orbitals in the vicinity of the $Z = N = 30$ SD shell gaps (see Fig. 1) and comparing calculated effective alignments i_{eff} with observed ones in the ^{58}Cu/^{60}Zn, ^{60}Zn/^{62}Zn, ^{58}Cu/^{62}Zn pairs (Fig. 3), it was found that the physical observables ($J^{(1)}$, $J^{(2)}$ and i_{eff}) are best described when the configurations $[21, 21]$ and $[22, 24]$ are assigned to the bands in ^{58}Cu and ^{62}Zn, respectively. The configuration $[21, 21]$ in ^{58}Cu is calculated to be energetically favored over a considerable spin range in both approaches and also in the cranked Hartree-Fock approach with Skyrme forces [8].

The experimental $J^{(1)}$ and $J^{(2)}$ moments of inertia of the ^{62}Zn band are somewhat better described in CRMF theory than in the CN model (see Figs. 2e,f). The fact that the last experimental point in $J^{(2)}$ is overestimated in the CRMF calculations is possibly due to an interaction between the occupied $[431]3/2^+$ and unoccupied $[431]1/2^+$ orbitals (see bottom panel of Fig. 1). One should note, however, that the configuration $[22, 24]$ in ^{62}Zn is not calculated as the lowest SD configuration. In the spin range of interest, its energy above the lowest SD solution is $\approx 1 - 1.5$ MeV in CRMF theory (see for example Ref. [20]) and $\approx 0.5 - 1.0$ MeV in the CN model. In Ref. [1], the ^{62}Zn configurations $[22, 22]$ and $[22, 23]$, which are calculated lowest in energy, were considered instead. However, especially when compared with the band in ^{60}Zn, it becomes evident that these configurations do not provide

a satisfactory description of the observed properties of SD band in ^{62}Zn. The configuration with only one neutron hole in the $f_{7/2}$ orbital can be excluded for similar reasons but also because its signature partner is calculated degenerate in energy contrary to experiment where no signature partner band has been observed so far.

The calculated high energy of the configuration assigned to the observed band in ^{62}Zn suggests that the parameterizations used might not be optimal with respect of description of single-particle energies in the vicinity of the SD shell gaps. Note, however, that the CN model and CRMF theory with three different forces indicate the same group of orbitals in the vicinity of the $N = Z = 30$ SD shell gap (see top panel of Fig. 1). In both approaches, the $N = Z = 30$ SD shell gap is primarily defined by the energy splitting between the [440]1/2 and [431]3/2 orbitals originating from the intruder $g_{9/2}$ subshell. Thus the lowering of the $g_{9/2}$ subshell by $\sim 0.5 - 1$ MeV will almost not affect the size of the $N = Z = 30$ SD shell gap but will bring the conf. [22, 24] in ^{62}Zn closer to the yrast line. Note that this will also make the $N = 38$ shell gap seen in Fig. 1 smaller due to the lowering of the [422]5/2 orbital. The observation of other SD structures in ^{62}Zn and neighboring nuclei will be essential to establish the ordering of single-particle levels around the $N = 30$ SD shell gap and to determine the accuracy with which existing theories describe the alignment properties of single-particle orbitals. This should help to clarify how the models should be further improved to give an even better description of the variety of rotational structures observed in this mass region.

As inferred from the analysis of effective alignments in Fig. 3, with the present configuration assignments, the lowest transition in the highly-deformed band of ^{58}Cu with the transition energy of 830 keV corresponds to a spin change of $11^+ \rightarrow 9^+$ and that the lowest transition in the SD band of ^{62}Zn with the transition energy of 1993 keV corresponds to a spin change of $20^+ \rightarrow 18^+$. Thus the bands in ^{58}Cu and ^{62}Zn are observed up to 23^+ and 30^+, respectively. The corresponding experimental values of $J^{(2)}$ and $J^{(1)}$ (under these spin assignments) are reproduced rather well in the calculations (see Fig. 2).

Considering the distribution of particles and holes over high- and low-j orbitals at low spin one obtains the 'maximum' spins of the configurations of the observed bands as $I = 29^+$ (^{58}Cu), $I = 36^+$ (^{60}Zn) and $I = 40^+$ (^{62}Zn). Thus the bands in ^{58}Cu and ^{60}Zn (^{62}Zn) are three (five) transitions away from the 'maximum' spin. Note however that the states of 'maximum' spin are collective due to the interaction between high- and low-j orbitals of

the $N = 3$ shell, i.e. these bands do not terminate in the usual sense. Even so, the properties of these bands are strongly influenced by the limited angular momentum content of their single-particle configurations. Indeed, several features of these bands are similar to those of smooth terminating bands observed in the $A \sim 110$ mass region [12] and in ^{62,64}Zn [2,22]. Such features are the smooth drop of the dynamic moment of inertia $J^{(2)}$ with increasing rotational frequency to values much lower than the kinematic moment of inertia $J^{(1)}$. Furthermore, a gradual drop of collectivity (i.e. a drop of transition quadrupole moment Q_t) is predicted with increasing spin for both kinds of bands, something which at present has been experimentally confirmed [2,21] only for smooth terminating bands. Indeed, in the $A \sim 60$ region, one can see the gradual transition from the smooth terminating bands in ^{62,64}Zn over the highly-deformed band in ^{58}Cu to the SD bands in ^{60,62}Zn. Calculations for a number of configurations in neighboring nuclei and in ^{68}Zn (see Ref. [23] for this nucleus) show that the above mentioned features are common for the SD and highly-deformed bands in the $A \sim 60 - 70$ mass region. Thus a rigid-rotor assumption ($J^{(1)} \approx J^{(2)}$) sometimes used in the analysis of SD bands is not valid in this mass region. Indeed, in line with previous studies [24], we can conclude that it is not so much the deformation (at $I = 0$) of a band which determines if it is rigid-rotor like or not but rather how far away the band is from its 'maximum' spin value. Therefore, it is in general much more difficult to find rigid-rotor like rotational bands in light nuclei because the 'maximum' spin within the yrast and near-yrast configurations is generally much lower than in heavier nuclei.

One should note the important role of the first two $f_{7/2}$ holes (in [303]7/2 orbitals at prolate shape) in the stabilization of high- and superdeformation for the nuclei around $Z = N = 30$. Their influence is twofold. First, they significantly contribute to the quadrupole moment (see Ref. [25]). In this respect the highly-deformed and SD bands in the $A \sim 60$ mass region are similar to the ones in the $A \sim 135$ mass region, where the proton $g_{9/2}$ holes play an important role in stabilization of superdeformation (see Ref. [26]). Second, the contribution to the 'maximum' spin of these $f_{7/2}$ holes is comparable with the contribution from the $g_{9/2}$ particles. For example, full alignment of two highest $f_{7/2}$ holes gives $6\hbar$, while full alignment of two lowest $g_{9/2}$ particle gives $8\hbar$ in angular momentum.

The SD and highly-deformed bands in the $A \sim 60$ mass region are characterized by very large transition energies reaching 3.2 MeV or more at the top of all three bands studied here. For these bands, the excitation energies drawn relative to rigid rotor reference appears

6

to provide the best measure of how well the theory describes the response of the nuclei to rotation as illustrated in the bottom panel of Fig. 4. Note, however, that since the pairing correlations are neglected in the calculations the comparison between theory and experiment should be made not with respect to the ground state but with respect to some high spin state. Indeed, in this kind of plot the difference between different approaches and different parameterizations of the RMF theory is more clearly seen compared with the plot of dynamic and kinematic moments of inertia (see Fig. 2). Comparing different results one can conclude that the best description of excitation energies within configurations at high spin is obtained within the CRMF theory with the NLSH and NL3 forces for ^{60,62}Zn while the band in ^{58}Cu is somewhat better described in the CN model. Concerning relative energies of different configurations (not shown in Fig. 4), none of the approaches give the configuration assigned to the SD band in ^{62}Zn as yrast with somewhat larger discrepancies in the CRMF than in the CN approach.

In conclusion, the cranked relativistic mean field theory and the configuration-dependent shell-correction approach with the cranked Nilsson potential have been used for a study of super- and highly-deformed rotational bands in the $A \sim 60$ mass region. The experimental observables like the dynamic moment of inertia $J^{(2)}$ and the transition quadrupole moments Q_t are well described by both approaches. Using the fact that the yrast SD band in ^{60}Zn is linked to the low-spin level scheme it was shown that by means of the effective alignment approach it is possible to establish absolute spin values for the unlinked highly-deformed and superdeformed bands in neighboring nuclei. Thus for the first time it becomes possible to compare theory with experiment in a direct way also for spin-dependent physical observables like kinematic moment of inertia, $J^{(1)}$, and excitation energies as a function of spin, $E(I)$, for superdeformed bands in the unpaired regime. It was found that a much lower value of the dynamic $J^{(2)}$ than the kinematic $J^{(1)}$ moment of inertia at high spin is rather general feature of SD and highly-deformed bands in this mass region.

REFERENCES

[1] C. E. Svensson et al., Phys. Rev. Lett. 79 (1997) 1233

[2] C. E. Svensson et al., Phys. Rev. Lett. 80 (1998) 2558

[3] I. Ragnarsson, in *Proceedings of the Workshop on the Science of Intense Radioactive Ion Beams*, edited by J. B. McClelland and D. J. Vieira (Los Alamos National Laboratory Report No. LA-11964-C, 1990), p. 199

[4] C. E. Svensson et al., submitted to Phys. Rev. Lett.

[5] I. Ragnarsson, Phys. Lett. B 264 (1991) 5

[6] I. Ragnarsson, Nucl. Phys. A 557 (1993) 167c

[7] A. V. Afanasjev, G. Lalazissis and P. Ring, Nucl. Phys. A 634 (1998) 395

[8] D. Rudolph et al., Phys. Rev. Lett. 80 (1998) 3018

[9] W. Koepf and P. Ring, Nucl. Phys. A 493 (1989) 61

[10] W. Koepf and P. Ring, Nucl. Phys. A 511 (1990) 279

[11] T. Bengtsson and I. Ragnarsson, Nucl. Phys. A 436 (1985) 14

[12] A. V. Afanasjev and I. Ragnarsson, Nucl. Phys. A 591 (1995) 387

[13] L. K. Karlsson, I. Ragnarsson and S. Åberg, Nucl. Phys. A, in press

[14] J. Dudek, W. Nazarewicz and P. Olanders, Nucl. Phys. A 420 (1984) 285

[15] A. V. Afanasjev, J. König and P. Ring, Nucl. Phys. A 608 (1996) 107

[16] P.-G. Reinhard et al., Z. Phys. A 323 (1986) 13

[17] G. A. Lalazissis, J. König and P. Ring, Phys. Rev. C 55 (1997) 540

[18] M. M. Sharma, M. A. Nagarajan and P. Ring, Phys. Lett. B 312 (1993) 377

[19] J. König and P. Ring, Phys. Rev. Lett. 71 (1993) 3079

[20] H. Madokoro and M. Matsuzaki, report nucl-th/9803058 v2

[21] R. Wadsworth et al., Phys. Rev. Lett. 80 (1998) 1174

[22] A. Galindo-Uribarri et al., Phys. Lett. B 422 (1998) 45

[23] M. Devlin et al., to be published

[24] I. Ragnarsson, Phys. Lett. B 199 (1987) 317

[25] J. Dobaczewski, report nucl-th/9801056

[26] A. V. Afanasjev and I. Ragnarsson, Nucl. Phys. A 608 (1996) 176
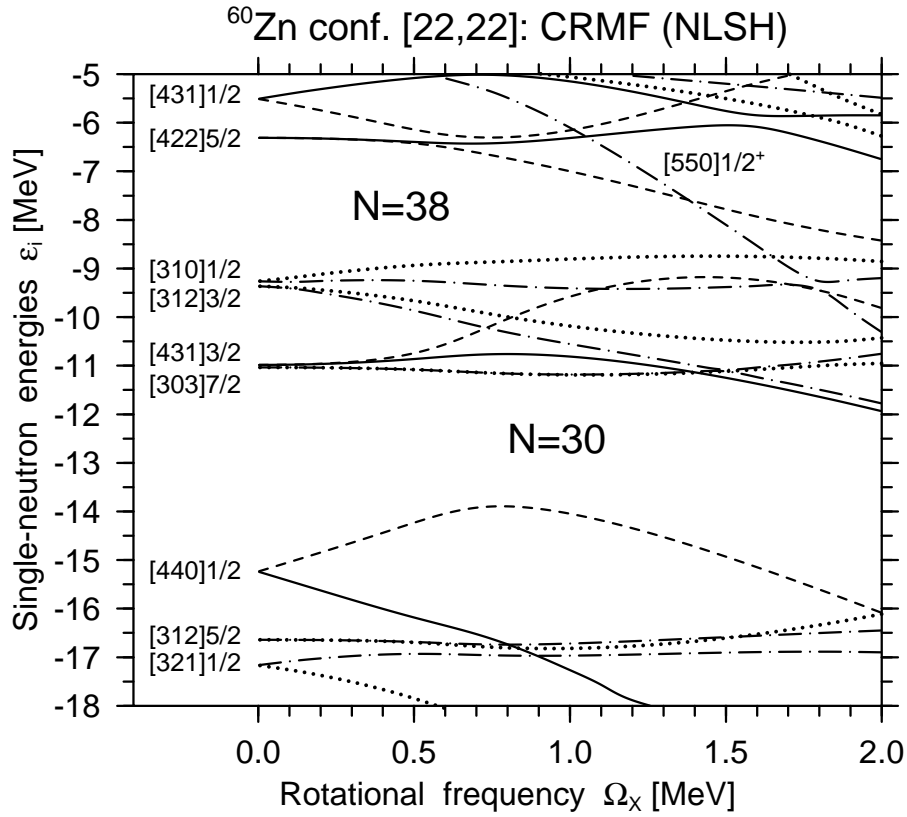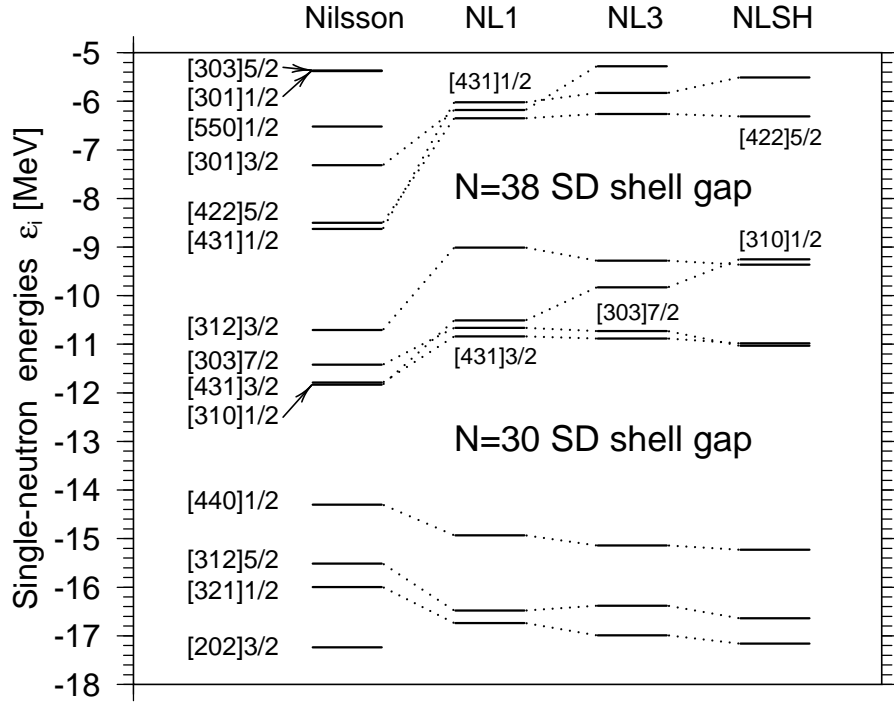
FIG. 1. Bottom panel: Neutron single-particle energies (routhians) in the self-consistent rotating potential as a function of the rotational frequency Ω_x calculated in CRMF theory with parameter set NLSH. They are given along the deformation path of the lowest SD configuration [22,22] in ^{60}Zn. Solid, short-dashed, dot-dashed and dotted lines indicate $(\pi = +, r = -i)$, $(\pi = +, r = +i)$, $(\pi = -, r = +i)$ and $(\pi = -, r = -i)$ orbitals, respectively. At $\Omega_x = 0.0$ MeV, the single-particle orbitals are labelled by the asymptotic quantum numbers $[Nn_z\Lambda]\Omega$ (Nilsson quantum numbers) of the dominant component of the wave function. Top panel: The single-particle states around the $N = 30$ SD shell gap calculated with the Nilsson potential and three parameterizations of RMF theory at the corresponding equilibrium deformations of the [22,22] configuration in ^{60}Zn at $\Omega_x = 0.0$ MeV. It is only in the CRMF calculations that the energies are absolute, in the Nilsson potential the energies are shifted so that the $N = 30$ SD shell gaps coincide roughly in both approaches. The relative single-particle energies are approximately the same for the protons as for the neutrons, but the absolute proton energies are higher because of the Coulomb energy. The fact that the spectrum is less dense in RMF theory than in the Nilsson potential is related to low effective mass $(m^*/m \approx 0.6)$ in RMF theory.
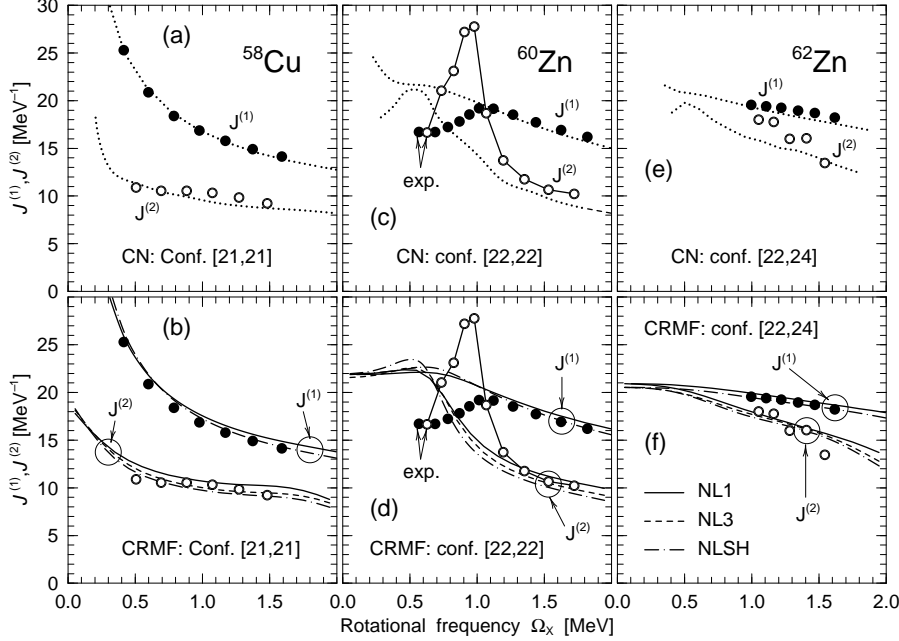

11

FIG. 2. Kinematic $J^{(1)}$ (unlinked solid circles) and dynamic $J^{(2)}$ (open circles) moments of inertia of observed bands versus the ones of assigned calculated configurations. The notation of lines is given in the figure.
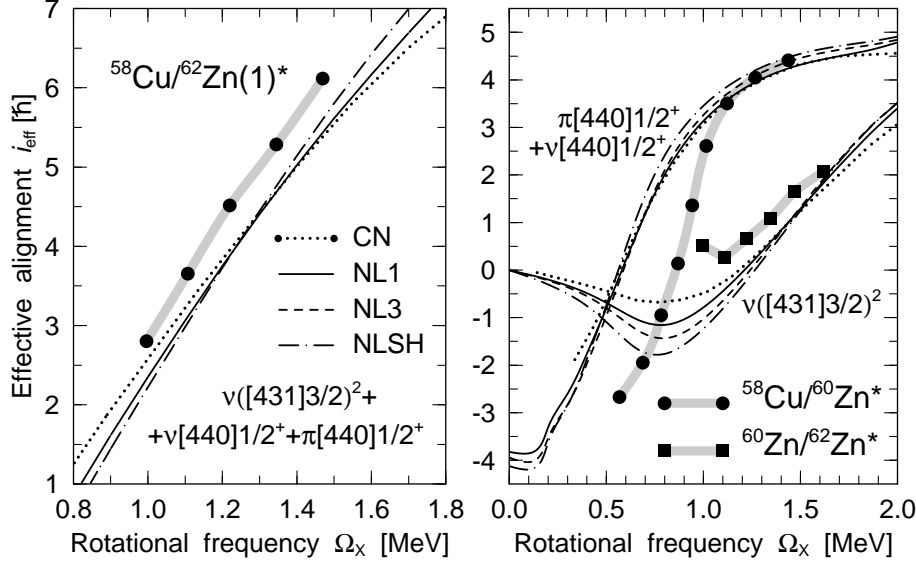

FIG. 3. Experimental (large solid symbols) and calculated (the notation of lines is given in the figure) effective alignments. The effective alignment between bands A and B is defined in Ref. [5] as $i_{eff}^{A,B}(\Omega_x) = I_B(\Omega_x) - I_A(\Omega_x)$. The band A in the lighter nucleus is taken as a reference, so the effective alignment measures the effect of additional particles. The experimental effective alignment between bands A and B is indicated as "A/B". The experimental i_{eff} values are shown at the transition energies of the band indicated by an asterisk (*). The compared configurations differ in the occupation of the orbitals indicated in the figure.
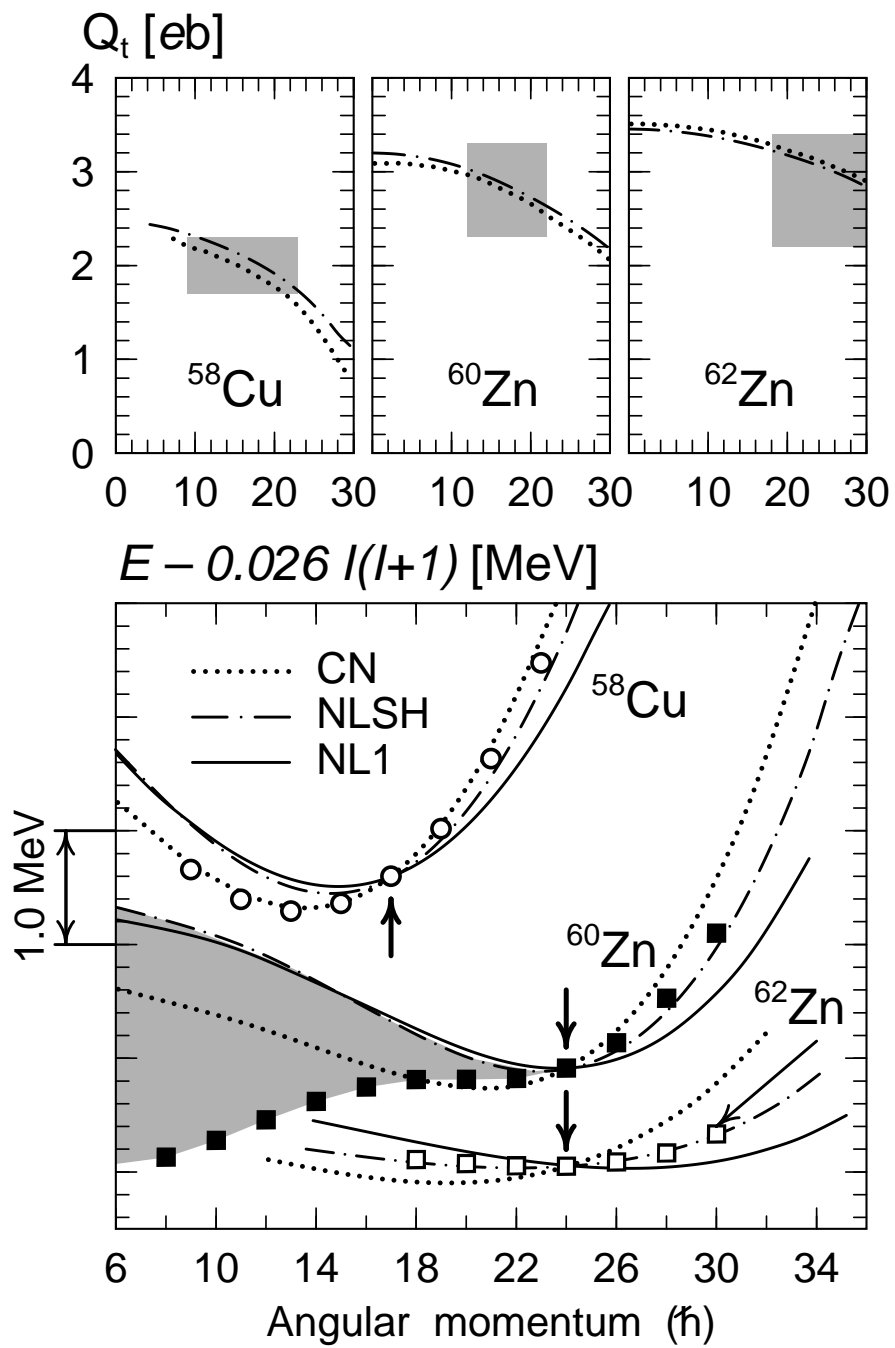
FIG. 4. Bottom panel: Calculated (lines) and experimental (symbols) bands shown relative to a rigid rotor reference. The energies of calculated states indicated by arrows are normalized to the corresponding experimental states. The shaded area is used to indicate the possible size of pairing correlations at low spin in the SD band of ^{60}Zn. The results with NL3 are rather close to the ones with NLSH, so for simplicity they are not shown. Top panels: Measured transition quadrupole moments Q_t (shaded boxes indicate the upper and lower limits of Q_t and the spin range where they have been measured) versus calculated ones. Since the Q_t values calculated with NL1 and NL3 differ from the ones with NLSH only by $\approx 2-3\%$, only the results of calculations with NLSH are shown.